# Breaking the Degrees-of-Freedom Limit of Holographic MIMO Communications: A 3-D Antenna Array Topology

Shuai S. A. Yuan, *Graduate Student Member, IEEE*, Jie Wu, *Member, IEEE*, Hongjing Xu, Tengjiao Wang, Da Li, *Member, IEEE*, Xiaoming Chen, *Senior Member, IEEE*, Chongwen Huang, *Member, IEEE*, Sheng Sun, *Senior Member, IEEE*, Shilie Zheng, *Member, IEEE*, Xianmin Zhang, *Member, IEEE*, Er-Ping Li, *Fellow, IEEE*, and Wei E. I. Sha, *Senior Member, IEEE*

***Abstract*—The performance of holographic multiple-input multiple-output (MIMO) communications, employing two-dimensional (2-D) planar antenna arrays, is typically compromised by finite degrees-of-freedom (DOF) stemming from limited array size. The DOF constraint becomes significant when the element spacing approaches approximately half a wavelength, thereby restricting the overall performance of MIMO systems. To break this inherent limitation, we propose a novel three-dimensional (3-D) antenna array that strategically explores the untapped vertical dimension. We investigate the performance of MIMO systems utilizing 3-D arrays across different multi-path scenarios, encompassing Rayleigh channels with varying angular spreads and the 3 rd generation partnership project (3GPP) channels. We subsequently showcase the advantages of these 3-D arrays over their 2-D counterparts with the same aperture sizes. As a proof of concept, a practical dipole-based 3-D array, facilitated by an electromagnetic band-gap (EBG) reflecting surface, is conceived, constructed, and evaluated. The experimental results align closely with full-wave simulations, and channel simulations substantiate that the DOF and capacity constraints of traditional holographic MIMO systems can be surpassed by adopting such a 3-D array configuration.**

***Index Terms*—3-D antenna array, channel capacity, degree of freedom, diversity measure, holographic multiple-input-multiple-output (MIMO) communications.**

Manuscript received 15 October 2023; revised 12 December 2023 and 24 January 2024; accepted 24 February 2024. Date of publication 30 May 2024; date of current version 15 August 2024. This work was supported by the National Natural Science Foundation of China under Grant 61975177, Grant U20A20164, and Grant 62201192. The review of this article was coordinated by Dr. Nghi H. Tran. *(Corresponding author: Wei E. I. Sha.)*

Shuai S. A. Yuan, Da Li, Chongwen Huang, Shilie Zheng, Xianmin Zhang, Er-Ping Li, and Wei E. I. Sha are with the College of Information Science and Electronic Engineering, Zhejiang University, Hangzhou 310027, China (e-mail: weisha@zju.edu.cn).

Jie Wu is with the Anhui Province Key Laboratory of Simulation and Design for Electronic Information System, Hefei Normal University, Hefei 230601, China.

Hongjing Xu and Tengjiao Wang are with Wireless Network Research Department, Huawei Technologies, Shanghai 201206, China.

Xiaoming Chen is with the School of Information and Communications Engineering, Xi'an Jiaotong University, Xi'an 710049, China.

Sheng Sun is with the School of Electronic Science and Engineering, University of Electronic Science and Technology of China, Chengdu 611731, China.

Digital Object Identifier 10.1109/TVT.2024.3372704

## I. Introduction

THE multiple-input-multiple-output (MIMO) technology, pivotal in wireless communications, has demonstrated substantial capacity enhancement across diverse scenarios, marking considerable success over the years [1], [2], [3]. In the pursuit of augmenting MIMO communication performance, several technologies have been developed. Some representative technologies include massive MIMO communications [4], [5], [6], [7], decoupling and decorrelation of MIMO arrays [8], [9], [10], [11], reconfigurable intelligent surface (RIS) aided MIMO communications [12], [13], and holographic MIMO communications [14], [15], [16], [17], [18], [19], [20], [21], [22]. Holographic MIMO communications, an advanced iteration of RIS, present promising avenues for research in the realm of highly adaptable antennas by skillfully harnessing electromagnetic (EM) waves [23], [24], [25], [26]. Notably, a holographic MIMO array can comprise a large amount of antennas within a compact aperture, and it has been substantiated to possess numerous advantages [27].

However, the primary challenge associated with holographic MIMO communications is the finite degrees-of-freedom (DOF) constrained by array size [28]. Given that a holographic MIMO array integrates a substantial number of antennas with sub-wavelength inter-element spacing within a confined area, a pronounced correlation emerges among the antennas, resulting in performance degradation. To compensate for such an impaired performance, an increase in array size is expected. Unfortunately, in practice, the array sizes at the base stations or vehicles are strictly confined due to wind drag, city planning, product requirements, etc. Hence, exceeding the DOF limit is imperative in further enhancing the performance of holographic MIMO.

In the pursuit of surpassing the DOF limit, it is necessary to make clear the fundamental limits of holographic MIMO communications. This analysis has been undertaken from dual perspectives–both information and electromagnetic (EM)–to provide a comprehensive understanding of the inherent limitations [29], [30], [31], [32], [33], [34], [35], [36], [37]. In a typical multi-path environment, the performance of a MIMO system depends on both the power gain and the DOF gain [2]. The power gain is known as the beamforming gain, which is

constricted by the aperture size of the array [38]. One famous argument is Hannan's limit [39], providing the closed-form expression of the radiation efficiency limit of antenna elements when more and more elements are placed into a constrained planar aperture. In addition to the power gain, the DOF gain usually attracts more attention when dealing with MIMO communications. The EM DOF of a MIMO system refers to the effective rank (the number of significant eigenvalues) of its correlation matrix [2], the number of scattering channels [40], or the number of available spatial EM modes [41], which characterizes the spatial-multiplexing performance of the MIMO system. The DOF of a MIMO system has been discussed based on various models, including the general scattering method [29], [40], [42], [43], [44], the Green's function method [17], [30], [45], [46], [47], the intuitive methods [41], [48], the plane-wave expansion model [14], [23], etc. These models are essentially equivalent but use different expansion bases of EM waves. As a summary, the EM DOF limit of an aperture-constrained MIMO system is considered to be only dependent on the surface area of the transmitting/receiving space [29], [47], or the average scattering cross-section [34], [35].

Therefore, one possible route to violate the DOF limit of holographic MIMO communications is to build a three-dimensional (3-D) array, which explores the additional volume available in the vertical dimension, and thus extra DOF. The performance of a 3-D array has been examined in line-of-sight (LOS) scenarios [49], [50], revealing marginal benefits at far field, but has not yet been explored in rich-scattering environments. Also, some similar concepts can be found in using the scatterers over the MIMO array for realizing the de-correlation (thus improving the DOF and capacity) [10], [11], and employing the stacked intelligent metasurfaces for advanced computation and signal processing tasks [51], [52]. As far as our knowledge extends, neither the concept of breaking the DOF limit by using the 3-D array nor the corresponding performance analyses have been discussed before. In this work, a novel 3-D array topology is proposed for breaking the DOF limit of holographic MIMO systems built with two-dimensional (2-D) arrays. The contributions of this paper can mainly be attributed to the following three aspects:

- The theoretical analyses of the MIMO performances of 3-D arrays based on the 3-D Clarke and Kronecker models; for example, comparing the performances of the 3-D and 2-D arrays with the same aperture size at different height differences, element spacings, and angular spreads.
- A practical 3-D antenna array enabled by an electromagnetic band-gap (EBG) reflecting surface is designed, fabricated, and measured as a proof of concept.
- Assessments of the MIMO performances of the practical 3-D array are conducted in both Rayleigh channels with varying angular spreads and 3 rd generation partnership project (3GPP) channels.

A comprehensive exploration of the properties of the 3-D array topology in various scenarios is presented in detail. The findings reveal that the 3-D array holds significant promise as a candidate for augmenting MIMO performance in the landscape of future wireless communications.

TABLE I
PARAMETERS AND VARIABLES USED IN THIS PAPER

| Names | Definitions |
|---|---|
| $\rho_{mn}$ | Correlation between the $n$th and $m$th antennas |
| $\Psi$ | Diversity measure of the MIMO array |
| $N_t$, $N_r$ | Number of the transmitting and receiving antennas |
| $h$ | Height difference in 3-D antenna array |
| $\mathbf{\Phi}$ | Correlation matrix |
| $e^{emb}$ | Embedded radiation efficiency |
| $\Omega$ | Solid angle |
| $\lambda_0$, $k_0$ | Free-space wavelength and wavenumber |
| $k_x$, $k_y$ | Wavenumber components along the $x$ and $y$ directions |
| $\mathbf{k}_\Omega$ | Wave vector along the $\Omega$ direction |
| $E(\Omega)$ | Far-field electric-field pattern |
| $\gamma$ | Total signal-to-noise ratio |
| $\sigma$ | Eigenvalue of the correlation matrix |
| $S_{mn}$ | S parameter between the port $n$ and port $m$ |

The rest of this paper is organized as follows. In Section II, the methodology of the 3-D array, and the tools for evaluating MIMO performance, i.e., the 3-D Clarke and Kronecker models, are introduced. Next, the theoretical analyses are carried out in Section III based on the two models. After that, the design, simulation, and experimental validation of a practical 3-D array, together with the discussion of its MIMO performances in Rayleigh and 3GPP channels, are presented in Section IV. Finally, some remarks and conclusions are given in Section V. Table I summarizes a list of the frequently used parameters and variables in this paper.

## II. METHODOLOGY

The diagrams of the traditional 2-D array topology and the proposed 3-D array topology are depicted in Fig. 1. Without loss of generality, a one-row array is set up along the $x$-axis to reduce the complexities of analysis and design. Rather than using the traditional 2-D planar array with a perfect electric conductor (PEC) reflector in Fig. 1(a), a height difference is introduced between the nearby antennas for realizing the 3-D array in Fig. 1(b). The lower antennas are close to the EBG surface while the upper antennas maintain a suitable height difference, which can be enabled by a well-designed EBG surface. In the 3-D array, the spatial differences between the array elements are not only along the transverse ($x$ and $y$) directions, but also along the longitudinal ($z$) direction.

Intuitively, the distance between the nearby antennas becomes larger because of the introduced height difference, and thus the spatial correlation between them will become lower (indicating a larger DOF) because the spatial correlation between two antennas is usually negatively correlated to the distance between them. From another perspective, the area of the oblique projection of a 3-D array on the transverse plane is always larger than the area of the aperture of a 2-D array, as illustrated in Fig. 2(a). The above indicates that the additional volume along the vertical dimension can be utilized for realizing an equivalently larger 2-D array.

Particularly, a remark regarding the far-field angular spectrum analysis is given, as shown in Fig. 2(b). The angular domain for propagating waves is defined as $k_x^2 + k_y^2 \leq k_0^2$, where $k_0$ is the free-space wavenumber, $k_x$ and $k_y$ are the wavenumber components along the $x$ and $y$ directions. Assuming a planar

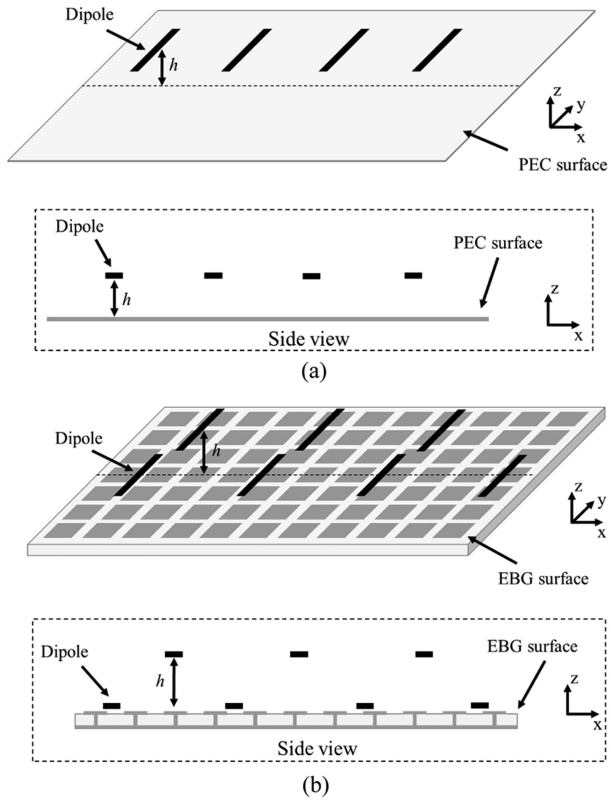


Fig. 1. Diagrams of the traditional 2-D antenna array and the proposed 3-D antenna array, where a one-row array is set up for demonstration. (a) Traditional 2-D antenna array over a PEC surface, where the heights of antennas are the same. (b) Proposed 3-D antenna array over an EBG surface and a height difference is introduced between the nearby antennas.

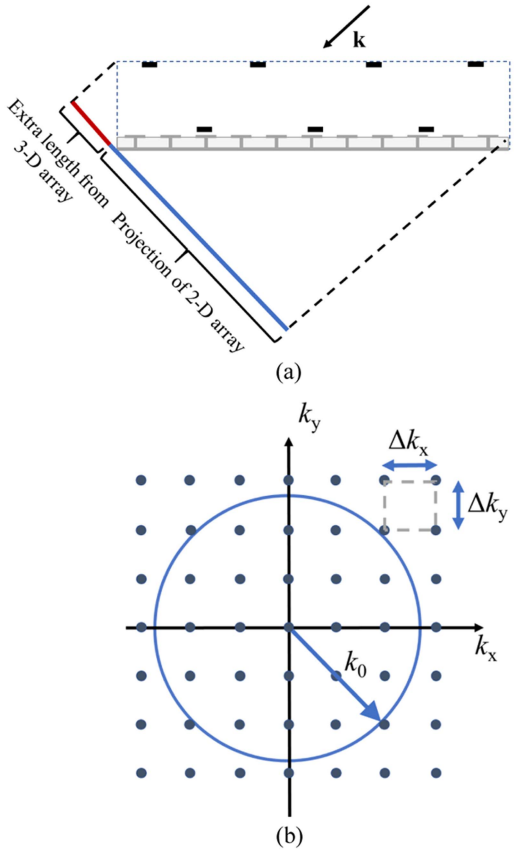


Fig. 2. Intuitive explanations of the benefits from a 3-D antenna array. (a) Under the incidence of a large-angle plane wave with the direction of $\mathbf{k}$, the 3-D array would have a larger projection area compared to the 2-D array. (b) In the angular spectrum analysis of the DOF limit, the blue circle with the radius of $k_0$ represents the available angular spectrum resource, $\Delta k_x$ and $\Delta k_y$ denote the resolutions along the $x$ and $y$ directions. The 3-D array would have better resolutions compared to the 2-D array at large angles.

surface with lengths $L_x$ and $L_y$ along the $x$ and $y$ directions, the resolutions of the beams generated by this surface along $k_x$ and $k_y$ at the far-field angular domain would be $\Delta k_x = 2\pi/L_x$ and $\Delta k_y = 2\pi/L_y$. Then, the DOF limit can be easily estimated by dividing the circular area (resource of angular domain $\pi k_0^2$) by the area of a dotted rectangle (resolution of a beam in angular domain $\Delta k_x \Delta k_y$) [41]. In this analysis, the resolutions $\Delta k_x = 2\pi/L_x$ and $\Delta k_y = 2\pi/L_y$ are the same for the beams towards different directions. In fact, the resolutions for beams towards large angles would be worse, since the resolutions would depend on the projection areas of the array along different directions, as shown in Fig. 2(a). Hence, the resource of angular domain is fixed for any far-field communication, while the 3-D array topology is expected to improve the resolutions of beams towards large angles, thus bringing more DOF for MIMO communications. To further explore the properties of 3-D array, including the benefits and drawbacks, the 3-D Clarke and Kronecker models are first used for characterizing their MIMO performances, as discussed below.

### A. 3-D Clarke Model

Based on the 3-D Clarke model [53], [54], the correlations between antennas in a Rayleigh fading environment can be analytically modeled for the theoretical analysis of MIMO performance. In the Clarke model, the antennas are simplified as

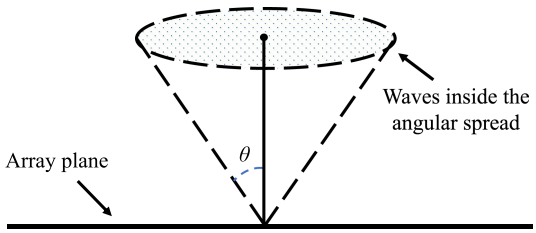


Fig. 3. Illustration of the angular spread, where the plane waves are uniformly distributed in an angular range characterized by $\theta$.

point receivers, and the incident waves are modeled as uniformly distributed far-field plane waves. The angular spread of the incident waves can be modified for approximately characterizing different scattering environments, as the spatial correlation is dominated by the angular spread, but not the specific distribution of the incident waves [55]. An illustration of angular spread is depicted in Fig. 3, and the mean incident angle is taken along the broadside of the array. The total signal received by one antenna can be regarded as the integral of these received plane waves along solid angles (with a sufficient number of plane waves). Therefore, one can easily formulate the correlation between the

two antennas at the positions $\mathbf{r}_m$ and $\mathbf{r}_n$ by

$$\rho_{nm} = \frac{1}{N}\int_{\Omega} \exp\left(j\mathbf{k}_{\Omega}\mathbf{r}_n - j\mathbf{k}_{\Omega}\mathbf{r}_m\right) \mathrm{d}\Omega, \tag{1}$$

where $N$ is the number of arriving plane waves, $\Omega$ represents the solid angles of the plane waves within the angular spread, and $\mathbf{k}_{\Omega}$ denotes the wave vector along the $\Omega$ direction. Then, the correlation matrix $\mathbf{\Phi}$ of the array can be obtained for evaluating the MIMO performance, i.e., the DOF and capacity. Complex Gaussian variables can be introduced for characterizing thermal noise, but will not affect the correlations.

DOF indicates the spatial multiplexing performance of a MIMO communication system; in (7.12) of reference [2], DOF is defined as the rank of correlation matrix, i.e., the number of significant eigenvalues. Physically, these eigenvalues are related to the EM eigenmodes generated from the array [56].

The DOF limit of a MIMO system is generally dependent on the size of array but not the antenna number, where the eigenvalues corresponding to the saturated antennas are too small to contribute to DOF [41]. Other than DOF, the diversity measure [1] is also frequently used for characterizing the spatial multiplexing performance [9], [30], [57], [58], also called effective DOF. Diversity measure $\Psi$, which can approximately represent the equivalent number of isolated antennas of a MIMO array, can be calculated by [57]

$$\Psi\left(\mathbf{\Phi}\right) = \left(\frac{\mathrm{tr}\left(\mathbf{\Phi}\right)}{\|\mathbf{\Phi}\|_F}\right)^2 = \frac{\left(\sum_i \sigma_i\right)^2}{\sum_i \sigma_i^2}, \tag{2}$$

where $\mathrm{tr}(\cdot)$ represents the trace operator and $\sigma_i$ is the $i$th eigenvalue of the correlation matrix $\mathbf{\Phi}$. From (2), we can find that both DOF and diversity can well characterize the limit of spatial multiplexing, since no more eigenvalues can contribute to the increase of diversity measure after reaching the limit. The concept of DOF is more physically intuitive compared to the diversity. However, the diversity would be more helpful to capacity estimation, since the number of equivalent isolated antennas is quite straightforward when characterizing a practical MIMO array. Both the DOF and diversity can be used for well capturing the performance limit of spatial multiplexing, i.e., the limited number of significant eigenvalues of correlation matrix. In this work, we choose to use the diversity measure due to its engineering convenience, and the diversity measure used here should also be distinguished from the antenna diversity for stabilizing wireless link. To avoid any confusion, we have clearly clarified the definitions of the DOF and diversity, since the definitions of these terms may be discrepant in different works or societies.

Furthermore, we evaluate the capacity of MIMO systems under the vertical-bell-labs-space-time (V-BLAST) architecture [2], where the transmitting side is ideal (the antennas are uncorrelated and their efficiencies are equal to 1). The channel matrix is unknown to the transmitters, and the transmitting power is equally allocated. This architecture allows us to focus on the characteristics of the array at the receiving side. The ergodic capacity incorporating antenna effects can be written as [59]

$$C = E\left\{\log_2\left[\det\left(\mathbf{I} + \frac{\gamma}{N_t}\mathbf{R}\mathbf{H}_w\mathbf{H}_w^H\right)\right]\right\}, \tag{3}$$

where $E$ represents the mathematical expectation, $^H$ is the Hermitian operator, the covariance matrix $\mathbf{R}$ equals $\mathbf{\Phi}$ in the Clarke model (ideal antenna efficiencies), and $\mathbf{I}$ is the identity matrix. Moreover, $N_t$ and $N_r$ are the number of transmitting and receiving antennas ($N_t = N_r$ is assumed here for the convenience of analysis), $\gamma$ is the fixed total signal-to-noise ratio (SNR), and the entries of $\mathbf{H}_w$ are independent and identically distributed (i.i.d.) complex Gaussian variables. Usually, the $\mathbf{H}_w$ is normalized by making $\|\mathbf{H}_w\|_F^2 = N_t N_r$ for fair comparisons [2], [60], where the $N_t N_r$ represents the array gain (or power gain) of the MIMO channel. This is a frequently used assumption in MIMO communications, the antennas are simplified as isotropic point sources, and the element spacing is an integer multiple of $\lambda_0/2$. Under this assumption, the array gain is simply equal to the number of antennas (assuming the antennas are lossless). However, the receiving array gain of an aperture-constrained array will not further increase when the element spacing becomes smaller than $\lambda_0/2$. Hence, the $\mathbf{H}_w$ is normalized by making $E\{\|\mathbf{H}_w\|_F^2\} = N_t N_r$ when the element spacing is larger than half wavelength, and making $E\{\|\mathbf{H}_w\|_F^2\} = N_t N_{\lambda_0/2}$ otherwise [17], [60], where $N_{\lambda_0/2}$ is the number of antennas at $\lambda_0/2$ element spacing.

### B. Kronecker Model

For practical antenna arrays, the deformation of radiation patterns and the decrease of radiation efficiencies caused by mutual coupling are required to be taken into consideration [59], [61], [62]. The covariance matrix $\mathbf{R}$ is constructed by the entry-wise product between the correlation matrix $\mathbf{\Phi}$ and the embedded efficiency matrix $\mathbf{\Xi}$, i.e.,

$$\mathbf{R} = \mathbf{\Phi} \circ \mathbf{\Xi}. \tag{4}$$

The correlation matrix incorporating mutual coupling is [63]

$$\mathbf{\Phi} = \begin{bmatrix} 1 & \rho_{12} & \cdots & \rho_{1N_r} \\ \rho_{21}^*, & 1 & \cdots & \rho_{2N_r} \\ \vdots & \vdots & \ddots & \vdots \\ \rho_{N_r1}^* & \rho_{N_r2}^*, & \cdots & 1 \end{bmatrix}, \tag{5}$$

where

$$\rho_{mn} = \frac{\oint G_{mn}(\Omega)\mathrm{d}\Omega}{\sqrt{\oint G_{mm}(\Omega)\mathrm{d}\Omega}\sqrt{\oint G_{nn}(\Omega)\mathrm{d}\Omega}}, \tag{6}$$

with

$$G_{mn}(\Omega) = \kappa E_{\theta m}(\Omega)E_{\theta n}^*(\Omega)P_{\theta}(\Omega) + E_{\phi m}(\Omega)E_{\phi n}^*(\Omega)P_{\phi}(\Omega), \tag{7}$$

$E_{\theta}(\Omega)$ and $E_{\phi}(\Omega)$ are the $\theta-$ and $\phi-$polarized embedded radiation patterns, $P(\Omega)$ is the angular power spectrum, and $\kappa$ is the cross-polarization discrimination (XPD). The XPD is taken as 1 (polarization-balanced), and $P(\Omega)$ could be used for characterizing different angular spreads. The embedded efficiency

[1] Antenna diversity is a scheme that sends multiple copies of a signal to improve the reliability of data reception. The diversity measure here works as an indicator for the performance of MIMO spatial multiplexing, but can also be regarded as a measurement of antenna diversity, since they are closely related. For example, if the antennas are highly correlated, they are equivalent to much fewer independent antennas when using antenna diversity.

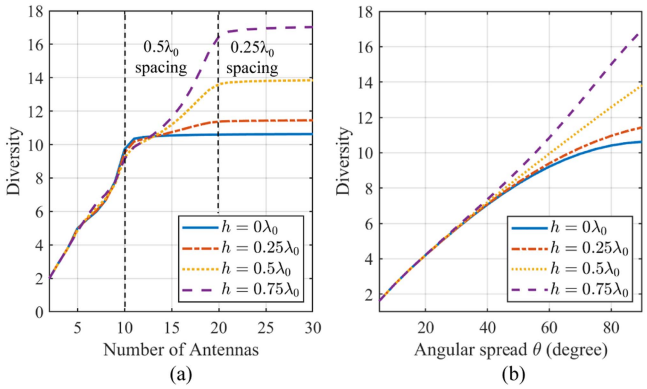


Fig. 4. Diversity measure based on the 3-D Clarke model, and the array length is fixed as $5\lambda_0$. (a) Diversities of the 3-D arrays with different $h$ and antenna numbers. (b) Diversities of the 3-D arrays with different $h$ and angular spreads, where the antenna number is fixed as 25.

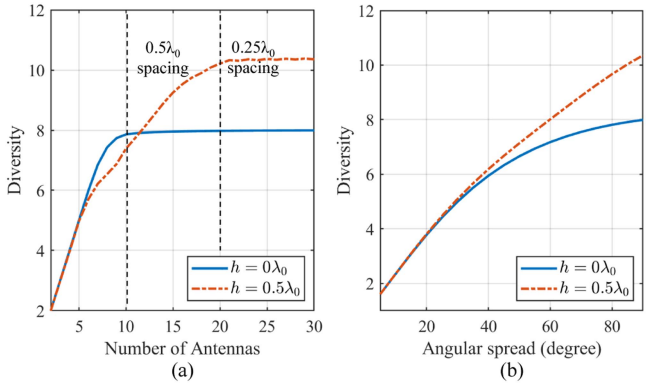


Fig. 5. Diversity measure based on the Kronecker model, and the array length is fixed as $5\lambda_0$. (a) Diversities of the 3-D arrays when $h = 0$ and $h = 0.5\lambda_0$. (b) Diversities of the 3-D arrays with different $h$ and angular spreads, where the antenna number is fixed as 25.

matrix $\boldsymbol{\Xi}$ is

$$\boldsymbol{\Xi} = \sqrt{\mathbf{e}}\sqrt{\mathbf{e}}^{T}, \tag{8}$$

with

$$\mathbf{e} = \left[e_1^{emb}, e_2^{emb}, \ldots, e_{N_r}^{emb}\right]^T, \tag{9}$$

where the embedded radiation efficiency of the $n$th antenna is calculated by the $S$ parameters assuming negligible ohmic loss [64]

$$e_n^{emb} = 1 - |S_{1n}|^2 - |S_{2n}|^2 - \cdots - |S_{N_r n}|^2. \tag{10}$$

In the characterization of practical antenna arrays, the power coupled to other ports is not regarded as the radiated power [65].

## III. Theoretical Analysis

We commence with the foundational Clarke model, wherein antennas are approximated as isotropic point sources, and mutual couplings are disregarded. In this section, the lengths of all the arrays are fixed as $5\lambda_0$, and a height difference $h$ is introduced between the nearby antennas for realizing 3-D array (see Fig. 1), and the 3-D array will degenerate into a 2-D array when $h = 0$. The diversities of 3-D arrays in different scenarios are investigated and presented in Fig. 4. In Fig. 4(a), it can be observed that the diversity in 2-D case ($h = 0$) will not further increase when element spacing reaches nearly $0.5\lambda_0$, which is the fundamental DOF limit of conventional holographic MIMO communications. However, the limit can be surpassed when a height difference between the nearby antennas is introduced, and the diversity keeps increasing until nearly $0.25\lambda_0$ element spacing. Moreover, the diversities under different angular spreads are presented in Fig. 4(b), where the increment of diversity brought by the 3-D configuration is positively related to the angular spread. The Kronecker model can be used for taking into account the distorted antenna radiation patterns. Rather than using the ideal isotropic radiation patterns, we first take into account the distortion of radiation patterns due to the 3-D antenna array topology, where the radiation patterns of the lower and upper antennas would be different. With a large height difference, side lobes are almost unavoidable for upper antennas according to the antenna array theory [38]. A $0.5\lambda_0$ height difference is taken here for balancing the antenna performance and DOF benefits, which is acceptable for a practical MIMO array. The radiation patterns of the upper and lower antennas are exported for performing the theoretical analyses here. The corresponding antenna designs and radiation patterns can be found in Figs. 8(b)–(c) and 11.

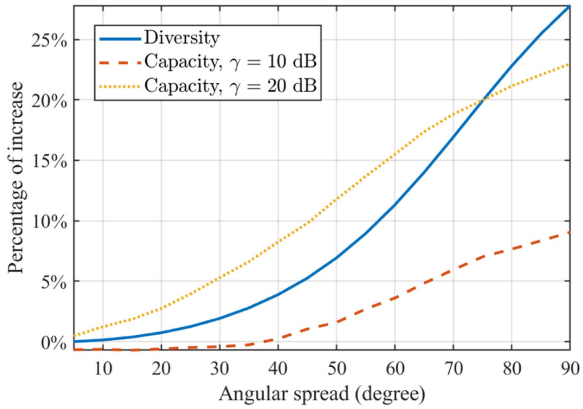


Fig. 6. Compared to using the 2-D array with the same aperture size, the percentages of increases in diversity and capacity by using the 3-D array.

Based on the Kronecker model, the diversities of 3-D arrays are calculated and presented in Fig. 5, showing that the DOF limit can be broken by using the 3-D configuration, and the increment brought by the 3-D array is largely dependent on the angular spread. It should be noticed that the diversities of 3-D arrays could be slightly lower than that of 2-D arrays without enough antennas, as shown in Fig. 5(a). In this situation, the performance of the 2-D array is close to saturation, while the 3-D array is still not well spatially sampled. The performance limit should always be reached or exceeded with a sufficient antenna number (i.e., holographic MIMO), and there may be few benefits from the 3-D array when the antenna number is not enough. For a better illustration, we plot the percentage of increases in diversity and capacity brought by the 3-D array compared to the 2-D array with the same aperture size in Fig. 6.

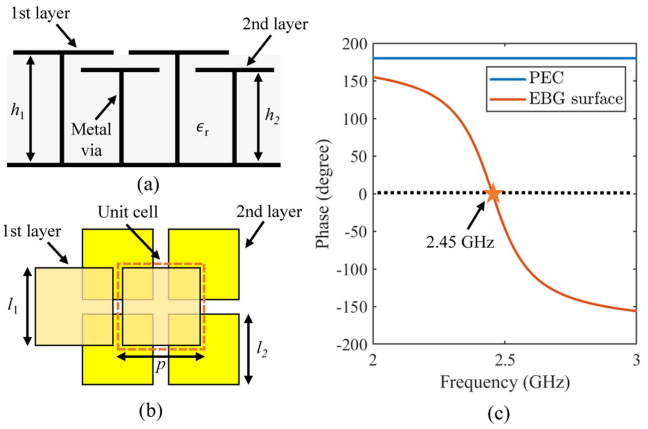


Fig. 7. Unit cell of the EBG surface for enabling the proposed 3-D array topology. (a) Side view of the double-layer EBG units, $h_1 = 1.83$ mm, $h_2 = 1.57$ mm. The relative dielectric constant of the substrate is $\epsilon_r = 2.2$. (b) Top view of the double-layer EBG units, $l_1 = 10.5$ mm, $l_2 = 9.5$ mm, $p = 11$ mm. (c) Reflecting phase of the EBG surface obtained from full-wave simulations, and a 0° reflecting phase can be realized at 2.45 GHz.

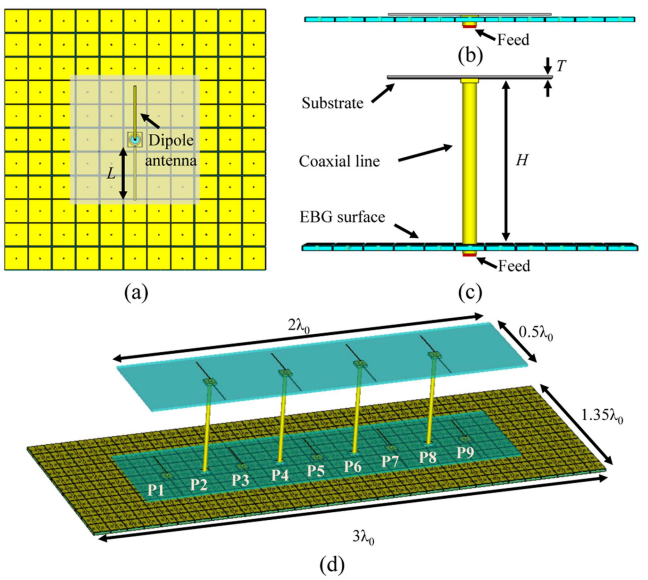


Fig. 8. Configuration of the 3-D antenna array. (a) Top view of a single antenna element, $L = 48$ mm. (b) Side view of the lower antenna element. (c) Side view of the upper antenna element, $H = 61$ mm, $T = 1.57$ mm. (d) Perspective view of the 3-D antenna array.

Theoretically, i.e., ideal decouplings are made, the diversity can be increased by 27%, and the capacity can be increased by 9% ($\gamma = 10$ dB) and 22.5% ($\gamma = 20$ dB) in an isotropic multi-path environment (angular spread is 90°). In practical applications, the angular spread may become smaller. When the angular spread is 60°, the diversity can still be increased by 12%, and the capacity can be increased by 4% ($\gamma = 10$ dB) and 15.5% ($\gamma = 20$ dB). Hence, the theoretical analyses put forth in this study strongly suggest that the proposed 3-D configuration successfully transcends the DOF limit, showcasing its potential application for enhancing capacity across a multitude of scenarios.

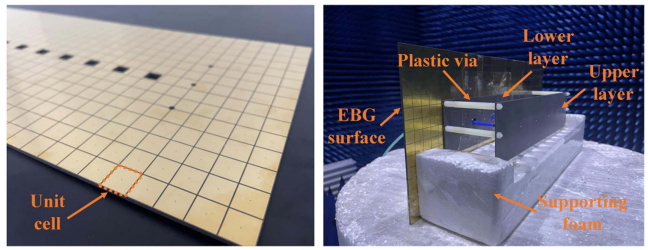


Fig. 9. Fabricated samples and experimental setup. (a) Fabricated EBG surface. (b) Fabricated 3-D antenna array and testing environment.

## IV. Numerical and Experimental Verifications

### A. Design of the 3-D Array

As a proof of concept, a practical 3-D array enabled by an EBG surface is designed for verifying the above theoretical analyses. To create the $0.5\lambda_0$ height difference while maintaining acceptable antenna performances, a 0° reflecting phase should be introduced by using the EBG surface at the working frequency. The design of EBG surfaces has been well discussed in literature [66], and a double-layer EBG surface is used here for realizing the desired functions [67]. The diagram of the utilized EBG structure is plotted in Fig. 7(a)–(b), and a 0° reflecting phase can be realized at 2.45 GHz in Fig. 7(c). To reduce the complexities of design, simulation, and fabrication, a microstrip dipole antenna is used here for facilitating the procedure of verification, as shown in Fig. 8(a). The full-wave models of the isolated upper and lower antennas are presented in Fig. 8(a)–(c), and a perspective view of the constructed 3-D array can be found in Fig. 8(d). Furthermore, the proposed 3-D array in Fig. 8(d) is fabricated and fully measured, the fabricated samples and experimental setup are demonstrated in Fig. 9.

### B. Numerical and Experimental Results of the 3-D Array

*1) Isolated Antenna:* The reflection coefficients and far-field radiation patterns of the isolated upper and lower antennasare first investigated, as shown in Fig. 10. The simulated and measured results agree well with each other, and the reflection coefficients are below −10 dB near the designed working frequency, which fulfills the requirements for array elements. Moreover, the electric-field patterns of the isolated antennas at far field (reference distance is taken as 1 m) are demonstrated in Fig. 11. It can be observed that the lower antenna maintains a regular radiation pattern [68], while the upper antenna has side lobes due to the introduced $0.5\lambda_0$ height difference. The side lobes in the upper antenna are almost inevitable, since its radiation pattern can be regarded as the end-fire radiation of a two-element in-phase array with $1\lambda_0$ distance. To create a larger height difference, directly increasing the height difference is detrimental to radiation patterns; however, a multilayer 3-D array would be more feasible. Moreover, the performances of antennas in the 3-D array can be further improved by the antenna and decoupling designs.

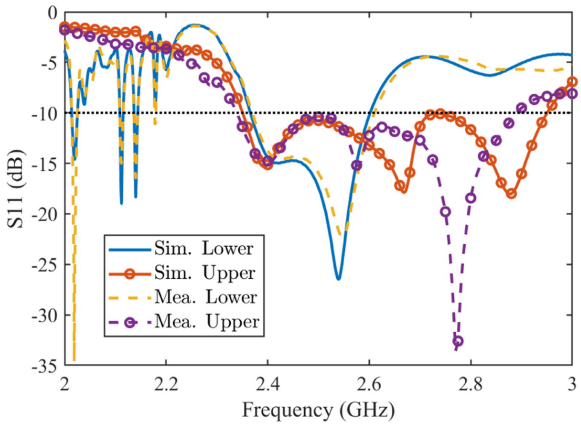


Fig. 10. Simulated and measured reflection coefficients of the isolated lower and upper antennas.

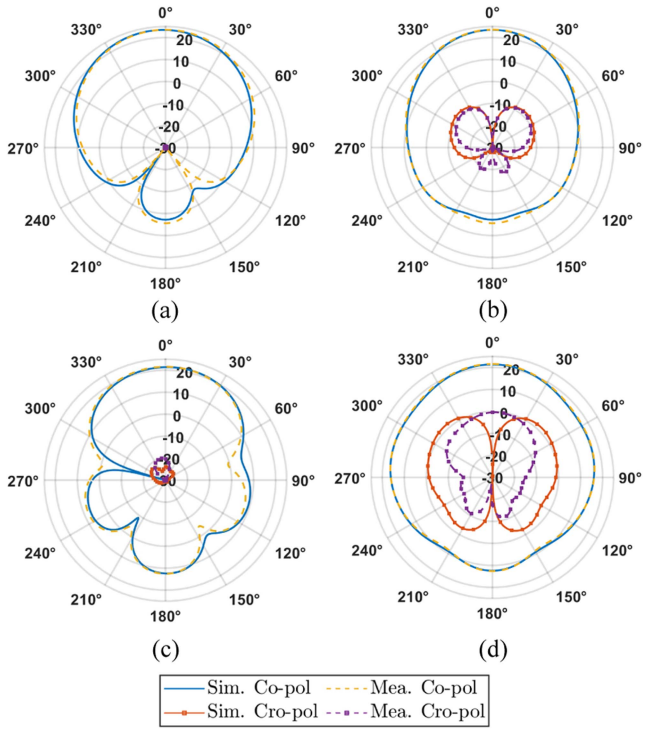


Fig. 11. Simulated and measured electric-field patterns of the isolated lower and upper antennas at far field (reference distance is taken as 1 m), and the unit is dB(V/m). The "Co-pol" and "Cro-pol" represent the co-polarized and cross-polarized patterns, respectively. (a)–(b) E-plane and H-plane patterns of the lower antenna. (c)–(d) E-plane and H-plane patterns of the upper antenna.

*2) Antennas in the 3-D Array:* The $S$ parameters and embedded radiation patterns of the antennas in a practical 3-D array are simulated and measured. Specifically, the embedded radiation pattern of one antenna in the array is obtained by exciting this antenna while making all the other antennas well-matched. The results of the first five antennas, i.e., P1–P5 in Fig. 8(d), are given considering the symmetric structure of 3-D array. The simulated and measured reflection coefficients are plotted and compared in Fig. 12. Near the desired frequency, the reflection coefficients are mostly below $-10$ dB, some deviations can be attributed to the fabrication and measurement errors. In Fig. 13, the simulated and measured embedded radiation patterns of the antennas in the 3-D array are given, where some parts of radiation patterns are deformed due to the mutual coupling at small element spacings.

From the perspective of beamforming, the 3-D array will have better gain than the 2-D array especially at large scanning angles, because the corresponding projection area is larger. The gain limit of a 2-D array is given by [38]

$$G = \frac{4\pi A}{\lambda^2}\cos\theta_0, \tag{11}$$

where $A$ is the area of the array, and $\cos\theta_0$ represents the decrease of projection area due to the increase of $\theta_0$. The 3-D array is expected to have a larger projection area, especially at large scanning angles benefiting from the increased height, thus breaking the gain limit of the 2-D array at large angles, as shown in Fig. 14.

The embedded radiation efficiencies of the antennas are calculated from $S$ parameters according to (10), which are drawn and compared to the efficiencies in the 2-D arrays at different element spacings (i.e., different antenna numbers) in Fig. 15. It can be found that the efficiencies in the 3-D array are generally lower than that in the 2-D array at $0.4\lambda_0$ spacing, but higher than that in the 2-D array at $0.22\lambda_0$ spacing (with the same antenna number as the 3-D array). The latter indicates that Hannan's efficiency limit for a planar array [39] is in fact broken by introducing the height difference in the 3-D array.

### C. MIMO Performance

*1) $2\lambda_0$ Array in Rayleigh Channel:* With the above results, i.e., embedded radiation patterns and efficiencies, the diversity and capacity of the 3-D array can be calculated and compared to the 2-D arrays with the same aperture size by using (3–10). Three types of arrays with $2\lambda_0$ array length are first considered, including the proposed 3-D array, the 2-D array at $0.4\lambda_0$ element spacing (i.e., only the lower layer of the 3-D array), and the 2-D array at $0.22\lambda_0$ element spacing (with the same antenna number as the 3-D array). The results at different SNR levels ($\gamma = 10$ and 20 dB) are depicted in Fig. 16(a) and (b), and the arrows in the figures indicate the lines corresponding to the diversity and capacity. It can be observed that the increments of diversities and capacities are close to the theoretical analyses in Section III. To be specific, compared to the 2-D array, the diversity is increased by 33%, and the capacity is increased by 13% ($\gamma = 10$ dB) and 30% ($\gamma = 20$ dB) in isotropic multi-path environment. When the angular spread is 60°, the diversity is increased by 18%, and the capacity is increased by 9% ($\gamma = 10$ dB) and 19% ($\gamma = 20$ dB). Particularly, for a regular 2-D array, the diversity may only slightly increase due to the mutual coupling after reaching the DOF limit, but the efficiency will dramatically decrease following Hannan's limit [39]. Therefore, placing too many antennas into a constrained planar area will generally be harmful to capacity, as shown by the $0.22\lambda_0$ and $0.4\lambda_0$ spacing 2-D arrays in Fig. 16(a).

*2) $5\lambda_0$ Array in Rayleigh Channel:* We also investigate the performance of a larger 3-D array in Fig. 17, with the length

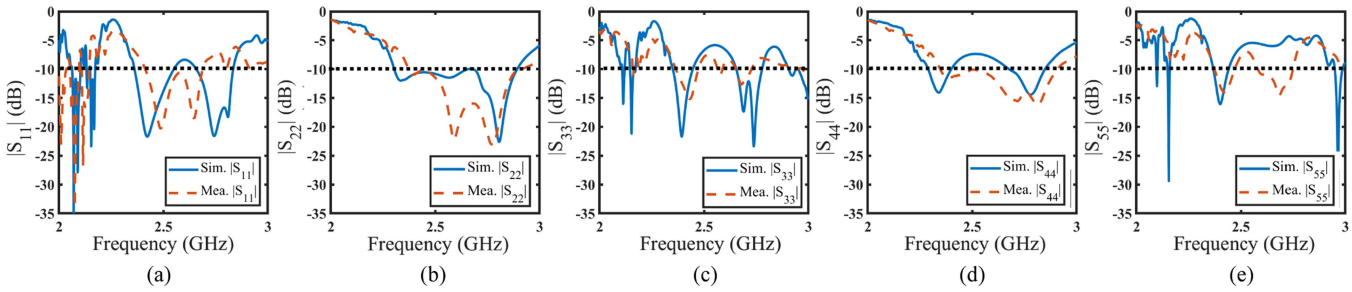


Fig. 12. Simulated and measured reflection coefficients of the antennas in a 3-D array. (a)–(e) Reflection coefficients of the antennas P1–P5.

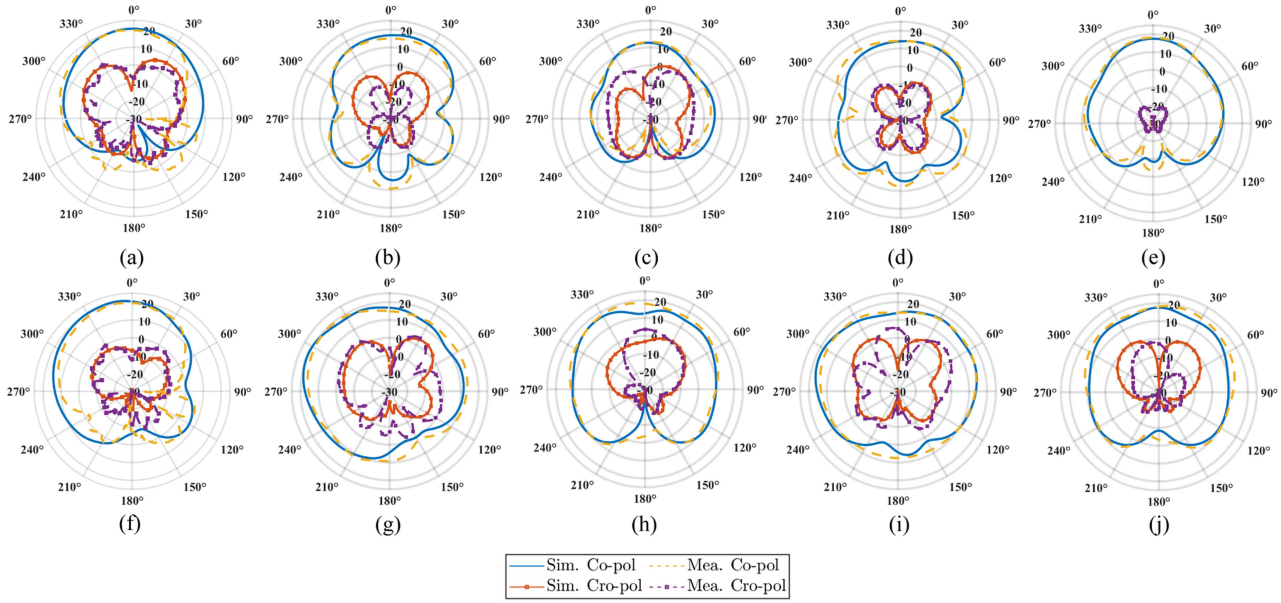


Fig. 13. Simulated and measured far-field patterns of the antennas in a 3-D array, the unit is dB(V/m). (a)–(e) E-plane patterns of the antennas P1–P5. (f)–(j) H-plane patterns of the antennas P1–P5.

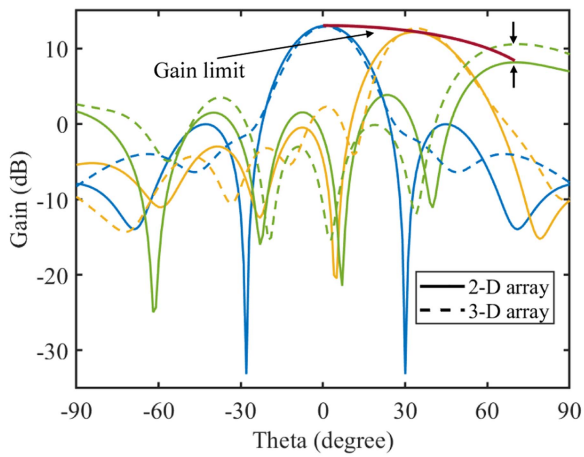


Fig. 14. Beamforming performances of the 2-D and 3-D arrays. The blue, orange, and green lines represent the gain patterns at the target beamforming angles of 0, 35, and 70 degrees, respectively. The solid and dotted lines represent the gain patterns of the 2-D and 3-D arrays. The red line denotes the theoretical gain limit of the 2-D array, which can be exceeded by the 3-D array at large scanning angles.

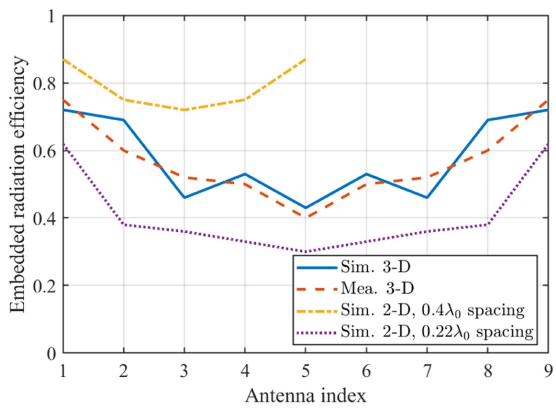


Fig. 15. Embedded radiation efficiencies of the antennas in different types of arrays.

of $5\lambda_0$ along the $x-$axis. In a large-scale array, the radiation patterns of the antennas in the middle region are similar [65], and the influence of edge antennas would be little. Compared

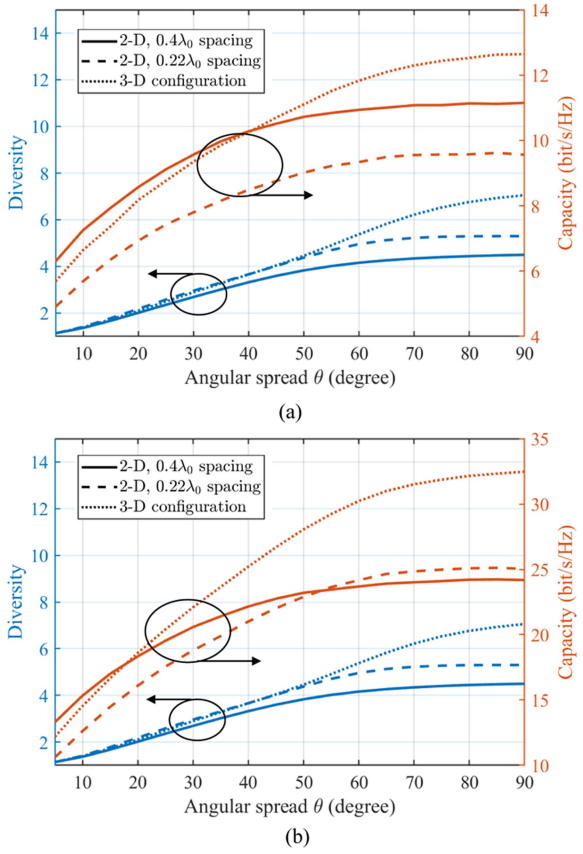


Fig. 16. Diversity and capacity benefits of the 3-D array compared to the 2-D array with the same aperture size, and the array length along the $x$-axis is $2\lambda_0$. (a) SNR $\gamma = 10$ dB. (b) SNR $\gamma = 20$ dB.

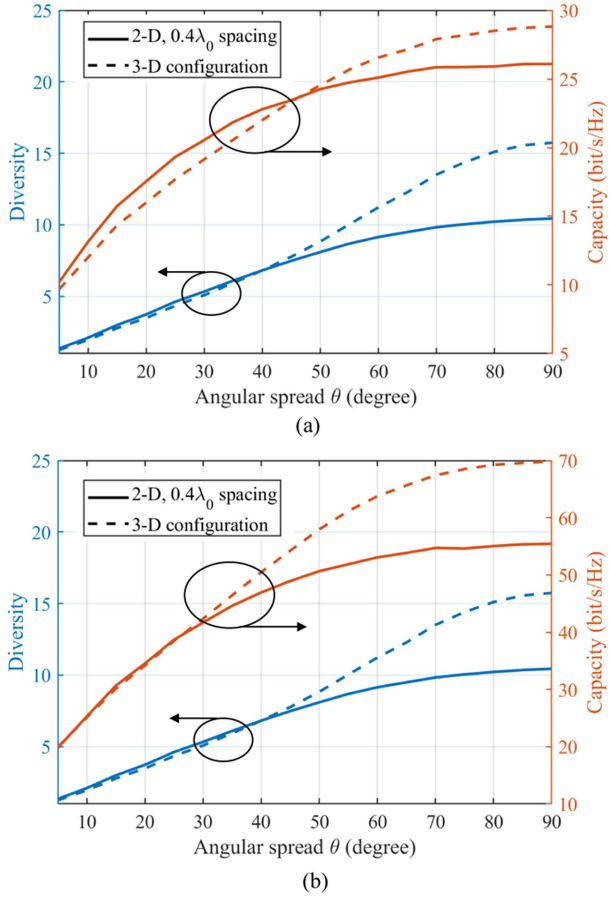


Fig. 17. Diversity and capacity benefits of the 3-D array compared to the 2-D array with the same aperture size, and the array length along the $x$-axis is $5\lambda_0$. (a) SNR $\gamma = 10$ dB. (b) SNR $\gamma = 20$ dB.

to the 2-D array at $0.4\lambda_0$ spacing, the capacity is increased by 12% ($\gamma = 10$ dB) and 26% ($\gamma = 20$ dB) in isotropic multi-path environment, and increased by 8% ($\gamma = 10$ dB) and 20% ($\gamma = 20$ dB) when the angular spread is 60°. In order to analyze the effects of mutual coupling, the percent of increase is drawn in Fig. 18 similar to the theoretical analysis in Fig. 6. It can be observed that the increments of capacities are slightly larger than the theoretical analyses in Section III at large angular spreads, because the large-angle radiations are stronger (indicating more DOF benefits are brought by the 3-D array configuration). However, the mutual coupling will degrade the performance of the 3-D array at low SNR and small angular spreads (the capacity enhancement brought by the extra DOF is not significant), also bring troubles for beamforming.

It also should be noticed that the 3-D array provides marginal benefits over the 2-D array in far-field LOS scenarios [49], [50], which is in consistent with our analyses at small angular spreads. Therefore, the benefit of 3-D array is highly dependent on the SNR level, specific multi-path environments, and antenna designs (radiation patterns), while the obtained results reveal the superiorities of the 3-D array over the 2-D array with the same aperture size in many scenarios.

*3) 3GPP Channel:* To further investigate the MIMO performances of the 3-D array in practical communication environments rather than in the ideal Rayleigh channel, the

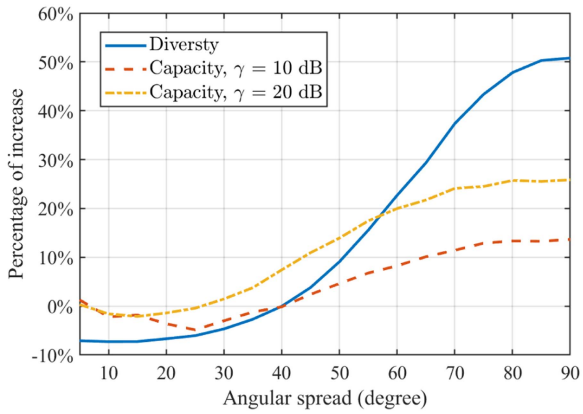


Fig. 18. Compared to using the 2-D array with the same aperture size, the percentages of increases in diversity and capacity by using the 3-D array configuration in a practical case.

open-source software QuaDRiGa is used for comparing the performances of 2-D and 3-D arrays in 3GPP channels [69]. Particularly, two single-cell scenarios are considered, including the *2-D 3GPP urban macro (UMa)* and *3-D 3GPP UMa* scenarios [69]. The configurations of the 3GPP models are

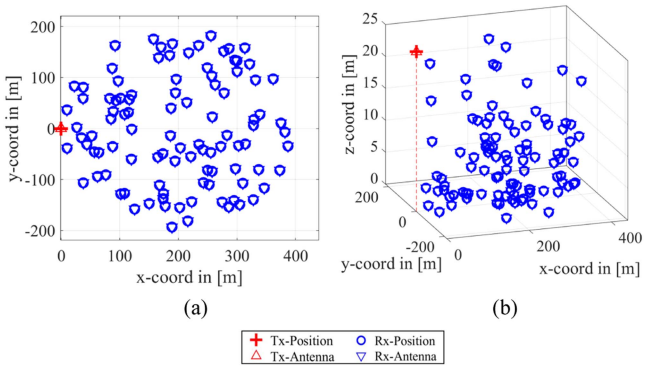


Fig. 19. Configurations of 2-D and 3-D 3GPP channels with 100 users. (a) 2-D 3GPP channel. (b) 3-D 3GPP channel.

TABLE II
BENEFITS OF THE 3-D ARRAY IN 3GPP CHANNELS

| Scenarios | 2-D array | 3-D array | Percent of increase |
|---|---|---|---|
| Diversity - 100 users (2-D 3GPP UMa) | 1.83 | 2.18 | 16% |
| Capacity - 100 users (2-D 3GPP UMa) | 18.50 | 21.08 | 13% |
| Diversity - 500 users (2-D 3GPP UMa) | 2.56 | 3.01 | 17% |
| Capacity - 500 users (2-D 3GPP UMa) | 21.13 | 23.80 | 13% |
| Diversity - 100 users (3-D 3GPP UMa) | 1.65 | 1.79 | 8% |
| Capacity - 100 users (3-D 3GPP UMa) | 16.84 | 18.17 | 8% |
| Diversity - 500 users (3-D 3GPP UMa) | 1.80 | 1.99 | 11% |
| Capacity - 500 users (3-D 3GPP UMa) | 17.76 | 19.02 | 7% |

demonstrated in Fig. 19, where the users (marked by blue circles) are distributed in a circular area with a radius of 200 m, and the base station (marked by a red cross) is placed on the left side of the circular area with the height of 25 m.

The users are arranged in accordance with the 3GPP assumptions [70], where 80% of them are situated indoors at different floor levels for the 3-D scenario and all set outdoors (1.5 m height) for the 2-D scenario. The embedded radiation patterns of the proposed $2\lambda_0$ 3-D array are imported as a transmitting array, while the users are set as omnidirectional antennas. After that, the channels of the paths created by different clusters are generated and summed for obtaining the wanted correlation matrix. Following (2-10), the diversity and capacity can be obtained for investigating the performances of 3-D arrays in geometry-based spatial correlation channels. The diversities and capacities ($\gamma = 20$ dB) with different numbers of users are calculated 50 times and averaged (each time the users are at different random positions), as presented in Table II. Compared to using the 2-D array with the same aperture size, the capacity can be increased by nearly 10% with 3-D array. Obviously, the benefits brought by the 3-D array in 3GPP channel are smaller than that in Rayleigh channel because of the smaller angular spread at the base station in 3GPP channels. Specifically, the azimuth angle spread at the base station side is regulated to be smaller than 104° (angular spread $\theta < 52°$) according to 3GPP TR 38.901 [70]. Therefore, when implementing a 3-D array, the specific settings should be carefully taken into consideration, including the array design, multi-path environment, SNR level, user density, etc.

## V. CONCLUSION

In this study, we successfully overcome the fundamental DOF limit in holographic MIMO communications by introducing a 3-D array topology. We systematically elucidate the principles behind the DOF limit and demonstrate the step-by-step utilization of the 3-D array topology to surpass this constraint, progressing from the ideal Clarke model to practical scenarios. Particularly, the benefits of 3-D array are illustrated from the perspectives of electromagnetics and beamforming. The numerical and experimental results further substantiate that, after reaching the DOF limit, the diversities and capacities of MIMO systems can be further improved by applying the 3-D topology. Furthermore, the performances of 3-D arrays in 3GPP channels are investigated, regarding the possible small angular spreads in practical implementations. Consequently, the 3-D array stands out as a promising candidate for bolstering MIMO performance across various scenarios in the future landscape of wireless communications.

Future endeavors will delve into exploring corresponding channel modeling and precoding technologies. Additionally, we aim to enhance hardware designs, incorporating advanced antenna and decoupling structures to improve radiation patterns and matching. These avenues of research will contribute to the ongoing advancement and optimization of holographic MIMO communication systems.

## REFERENCES

[1] E. Telatar, "Capacity of multi-antenna Gaussian channels," *Eur. Trans. Telecomm.*, vol. 10, no. 6, pp. 585–595, 1999.
[2] D. Tse and P. Viswanath, *Fundamentals of Wireless Communication*. Cambridge, U.K.: Cambridge Univ. Press, 2005.
[3] A. J. Paulraj, D. A. Gore, R. U. Nabar, and H. Bolcskei, "An overview of MIMO communications–A key to gigabit wireless," *Proc. IEEE*, vol. 92, no. 2, pp. 198–218, Feb. 2004.
[4] E. G. Larsson, O. Edfors, F. Tufvesson, and T. L. Marzetta, "Massive MIMO for next generation wireless systems," *IEEE Commun. Mag.*, vol. 52, no. 2, pp. 186–195, Feb. 2014.
[5] E. Björnson, L. Sanguinetti, H. Wymeersch, J. Hoydis, and T. L. Marzetta, "Massive MIMO is a reality–what is next?: Five promising research directions for antenna arrays," *Digit. Signal Process.*, vol. 94, pp. 3–20, 2019.
[6] J. Hoydis, S. Ten Brink, and M. Debbah, "Massive MIMO in the UL/DL of cellular networks: How many antennas do we need?," *IEEE J. Sel. Areas Commun.*, vol. 31, no. 2, pp. 160–171, Feb. 2013.
[7] Z. Wang et al., "Extremely large-scale MIMO: Fundamentals, challenges, solutions, and future directions," *IEEE Wireless Commun.*, early access, Apr. 10, 2023, doi: 10.1109/MWC.132.2200443.
[8] K.-L. Wu, C. Wei, X. Mei, and Z.-Y. Zhang, "Array-antenna decoupling surface," *IEEE Trans. Antennas Propag.*, vol. 65, no. 12, pp. 6728–6738, Dec. 2017.
[9] S. Zhang, X. Chen, and G. F. Pedersen, "Mutual coupling suppression with decoupling ground for massive MIMO antenna arrays," *IEEE Trans. Veh. Technol.*, vol. 68, no. 8, pp. 7273–7282, Aug. 2019.
[10] X. Chen et al., "Simultaneous decoupling and decorrelation scheme of MIMO arrays," *IEEE Trans. Veh. Technol.*, vol. 71, no. 2, pp. 2164–2169, Feb. 2022.

[11] Y. Wang et al., "Improvement of diversity and capacity of MIMO system using scatterer array," *IEEE Trans. Antennas Propag.*, vol. 70, no. 1, pp. 789–794, Jan. 2022.

[12] W. Tang et al., "MIMO transmission through reconfigurable intelligent surface: System design, analysis, and implementation," *IEEE J. Sel. Areas Commun.*, vol. 38, no. 11, pp. 2683–2699, Nov. 2020.

[13] C. Huang, A. Zappone, G. C. Alexandropoulos, M. Debbah, and C. Yuen, "Reconfigurable intelligent surfaces for energy efficiency in wireless communication," *IEEE Trans. Wireless Commun.*, vol. 18, no. 8, pp. 4157–4170, Aug. 2019.

[14] L. Wei et al., "Multi-user holographic MIMO surfaces: Channel modeling and spectral efficiency analysis," *IEEE J. Sel. Topics Signal Process.*, vol. 16, no. 5, pp. 1112–1124, Aug. 2022.

[15] J. An et al., "Stacked intelligent metasurfaces for efficient holographic MIMO communications in 6G," *IEEE J. Sel. Areas Commun.*, vol. 41, no. 8, pp. 2380–2396, Aug. 2023.

[16] L. Wei et al., "Tri-polarized holographic MIMO surfaces for near-field communications: Channel modeling and precoding design," *IEEE Trans. Wireless Commun.*, vol. 22, no. 12, pp. 8828–8842, Dec. 2023.

[17] S. S. A. Yuan, X. Chen, C. Huang, and W. E. I. Sha, "Effects of mutual coupling on degree of freedom and antenna efficiency in holographic MIMO communications," *IEEE Open J. Antennas Propag.*, vol. 4, pp. 237–244, 2023.

[18] Y. Zhang, J. Zhang, Y. Zhang, Y. Yao, and G. Liu, "Capacity analysis of holographic MIMO channels with practical constraints," *IEEE Wireless Commun. Lett.*, vol. 12, no. 6, pp. 1101–1105, Jun. 2023.

[19] O. T. Demir, E. Bjornson, and L. Sanguinetti, "Channel modeling and channel estimation for holographic massive MIMO with planar arrays," *IEEE Wireless Commun. Lett.*, vol. 11, no. 5, pp. 997–1001, May 2022.

[20] T. Gong et al., "Holographic MIMO communications: Theoretical foundations, enabling technologies, and future directions," *IEEE Commun. Surveys Tuts.*, vol. 26, no. 1, pp. 196–257, Firstquarter 2024, doi: 10.1109/COMST.2023.3309529.

[21] T. Gong et al., "Holographic MIMO communications with arbitrary surface placements: Near-field LoS channel model and capacity limit," *IEEE J. Sel. Areas Commun.*, vol. 42, no. 6, pp. 1549–1566, Jun. 2024.

[22] T. Gong, C. Huang, J. He, M. Di Renzo, M. Debbah, and C. Yuen, "A transmit-receive parameter separable electromagnetic channel model for LoS holographic MIMO," in *Proc. IEEE Glob. Commun. Conf.*, 2023, pp. 5701–5716.

[23] A. Pizzo, T. L. Marzetta, and L. Sanguinetti, "Spatially-stationary model for holographic MIMO small-scale fading," *IEEE J. Sel. Areas Commun.*, vol. 38, no. 9, pp. 1964–1979, Sep. 2020.

[24] J. An, C. Yuen, C. Huang, M. Debbah, H. V. Poor, and L. Hanzo, "A tutorial on holographic MIMO communications–Part I: Channel modeling and channel estimation," *IEEE Commun. Lett.*, vol. 27, no. 7, pp. 1664–1668, Jul. 2023.

[25] J. An, C. Yuen, C. Huang, M. Debbah, H. V. Poor, and L. Hanzo, "A tutorial on holographic MIMO communications–Part II: Performance analysis and holographic beamforming," *IEEE Commun. Lett.*, vol. 27, no. 7, pp. 1669–1673, Jul. 2023.

[26] J. An, C. Yuen, C. Huang, M. Debbah, H. V. Poor, and L. Hanzo, "A tutorial on holographic MIMO communications–Part III: Open opportunities and challenges," *IEEE Commun. Lett.*, vol. 27, no. 7, pp. 1674–1678, Jul. 2023.

[27] C. Huang et al., "Holographic MIMO surfaces for 6G wireless networks: Opportunities, challenges, and trends," *IEEE Wireless Commun.*, vol. 27, no. 5, pp. 118–125, Oct. 2020.

[28] A. Pizzo, T. L. Marzetta, and L. Sanguinetti, "Degrees of freedom of holographic MIMO channels," in *Proc. IEEE 21st Int. Workshop Signal Process. Adv. Wireless Commun.*, 2020, pp. 1–5.

[29] M. D. Migliore, "Horse (electromagnetics) is more important than horseman (information) for wireless transmission," *IEEE Trans. Antennas Propag.*, vol. 67, no. 4, pp. 2046–2055, Apr. 2019.

[30] S. S. A. Yuan, Z. He, X. Chen, C. Huang, and W. E. I. Sha, "Electromagnetic effective degree of freedom of an MIMO system in free space," *IEEE Antennas Wireless Propag. Lett.*, vol. 21, no. 3, pp. 446–450, Mar. 2022.

[31] Z. Wan, J. Zhu, Z. Zhang, L. Dai, and C.-B. Chae, "Mutual information for electromagnetic information theory based on random fields," *IEEE Trans Commun.*, vol. 71, no. 4, pp. 1982–1996, Apr. 2023.

[32] Z. Han, S. Shen, Y. Zhang, S. Tang, C.-Y. Chiu, and R. Murch, "Using loaded n-port structures to achieve the continuous-space electromagnetic channel capacity bound," *IEEE Trans. Wireless Commun.*, vol. 22, no. 11, pp. 7592–7605, Nov. 2023.

[33] W. Jeon and S.-Y. Chung, "Capacity of continuous-space electromagnetic channels with lossy transceivers," *IEEE Trans. Inf. Theory*, vol. 64, no. 3, pp. 1977–1991, Mar. 2018.

[34] M. Franceschetti, *Wave Theory of Information*. Cambridge, U.K.: Cambridge Univ. Press, 2017.

[35] M. Gustafsson and J. Lundgren, "Degrees of freedom and characteristic modes," *IEEE Antennas Propag. Mag.*, early access, May 22, 2023, doi: 10.1109/MAP.2024.3389451.

[36] D. Dardari and N. Decarli, "Holographic communication using intelligent surfaces," *IEEE Commun. Mag.*, vol. 59, no. 6, pp. 35–41, Jun. 2021.

[37] R. Li et al., "An electromagnetic information theory based model for efficient characterization of MIMO systems in complex space," *IEEE Trans. Antennas Propag.*, vol. 71, no. 4, pp. 3497–3508, Apr. 2023.

[38] C. A. Balanis, *Antenna Theory: Analysis and Design*. Hoboken, NJ, USA: Wiley, 2015.

[39] P. Hannan, "The element-gain paradox for a phased-array antenna," *IEEE Trans. Antennas Propag.*, vol. 12, no. 4, pp. 423–433, Jul. 1964.

[40] O. Bucci and G. Franceschetti, "On the degrees of freedom of scattered fields," *IEEE Trans. Antennas Propag.*, vol. 37, no. 7, pp. 918–926, Jul. 1989.

[41] S. S. A. Yuan et al., "Approaching the fundamental limit of orbital-angular-momentum multiplexing through a hologram metasurface," *Phys. Rev. Appl.*, vol. 16, 2021, Art. no. 064042.

[42] C. Ehrenborg, M. Gustafsson, and M. Capek, "Capacity bounds and degrees of freedom for MIMO antennas constrained by Q-factor," *IEEE Trans. Antennas Propag.*, vol. 69, no. 9, pp. 5388–5400, Sep. 2021.

[43] M. A. Jensen and J. W. Wallace, "Capacity of the continuous-space electromagnetic channel," *IEEE Trans. Antennas Propag.*, vol. 56, no. 2, pp. 524–531, Feb. 2008.

[44] A. S. Y. Poon, R. W. Brodersen, and D. N. C. Tse, "Degrees of freedom in multiple-antenna channels: A signal space approach," *IEEE Trans. Inf. Theory*, vol. 51, no. 2, pp. 523–536, Feb. 2005.

[45] S. S. A. Yuan, Z. He, S. Sun, X. Chen, C. Huang, and W. E. I. Sha, "Electromagnetic effective-degree-of-freedom limit of a MIMO system in 2-D inhomogeneous environment," *Electronics*, vol. 11, no. 19, 2022, Art. no. 3232.

[46] Y. Shen, Z. He, W. E. I. Sha, S. S. A. Yuan, and X. Chen, "Electromagnetic effective-degree-of-freedom prediction with parabolic equation method," *IEEE Trans. Antennas Propag.*, vol. 71, no. 4, pp. 3752–3757, Apr. 2023.

[47] R. Piestun and D. A. Miller, "Electromagnetic degrees of freedom of an optical system," *J. Opt. Soc. Amer. A-Opt. Image Sci. Vis.*, vol. 17, no. 5, pp. 892–902, 2000.

[48] D. A. Miller, "Communicating with waves between volumes: Evaluating orthogonal spatial channels and limits on coupling strengths," *Appl. Opt.*, vol. 39, no. 11, pp. 1681–1699, 2000.

[49] S. Hu, F. Rusek, and O. Edfors, "Beyond massive MIMO: The potential of data transmission with large intelligent surfaces," *IEEE Trans. Signal Process.*, vol. 66, no. 10, pp. 2746–2758, May 2018.

[50] X. Song and G. Fettweis, "On spatial multiplexing of strong line-of-sight MIMO with 3D antenna arrangements," *IEEE Wireless Commun. Lett.*, vol. 4, no. 4, pp. 393–396, Aug. 2015.

[51] J. An et al., "Stacked intelligent metasurface-aided MIMO transceiver design," *IEEE Wireless Commun.*, early access, Apr. 30, 2023, doi: 10.1109/MWC.013.2300259.

[52] J. An et al., "Stacked intelligent metasurfaces for efficient holographic MIMO communications in 6G," *IEEE J. Sel. Areas Commun.*, vol. 41, no. 8, pp. 2380–2396, Aug. 2023.

[53] R. H. Clarke, "A statistical theory of mobile-radio reception," *Bell Syst. Tech. J.*, vol. 47, no. 6, pp. 957–1000, Jul./Aug. 1968.

[54] R. H. Clarke and W. L. Khoo, "3-D mobile radio channel statistics," *IEEE Trans. Veh. Technol.*, vol. 46, no. 3, pp. 798–799, Aug. 1997.

[55] J. Andersen and K. Pedersen, "Angle-of-arrival statistics for low resolution antennas," *IEEE Trans. Antennas Propag.*, vol. 50, no. 3, pp. 391–395, Mar. 2002.

[56] D. A. Miller, "Waves, modes, communications, and optics: A tutorial," *Adv. Opt. Photon.*, vol. 11, no. 3, pp. 679–825, 2019.

[57] M. T. Ivrlac and J. A. Nossek, "Diversity and correlation in Rayleigh fading MIMO channels," in *Proc. IEEE 61st Veh. Technol. Conf.*, 2005, pp. 151–155.

[58] S. Verdu, "Spectral efficiency in the wideband regime," *IEEE Trans. Inf. Theory*, vol. 48, no. 6, pp. 1319–1343, Jun. 2002.

[59] X. Chen, P.-S. Kildal, J. Carlsson, and J. Yang, "MRC diversity and MIMO capacity evaluations of multi-port antennas using reverberation chamber and anechoic chamber," *IEEE Trans. Antennas Propag.*, vol. 61, no. 2, pp. 917–926, Feb. 2013.

[60] S. Loyka and G. Levin, "On physically-based normalization of MIMO channel matrices," *IEEE Trans. Wireless Commun.*, vol. 8, no. 3, pp. 1107–1112, Mar. 2009.
[61] P.-S. Kildal and K. Rosengren, "Correlation and capacity of MIMO systems and mutual coupling, radiation efficiency, and diversity gain of their antennas: Simulations and measurements in a reverberation chamber," *IEEE Commun. Mag.*, vol. 42, no. 12, pp. 104–112, Dec. 2004.
[62] S. Biswas, C. Masouros, and T. Ratnarajah, "Performance analysis of large multiuser MIMO systems with space-constrained 2-D antenna arrays," *IEEE Trans. Wireless Commun.*, vol. 15, no. 5, pp. 3492–3505, May 2016.
[63] X. Chen and S. Zhang, "Multiplexing efficiency for MIMO antenna-channel impairment characterisation in realistic multipath environments," *IET Microw. Antennas Propag.*, vol. 11, pp. 524–528, 2017.
[64] P.-S. Kildal, A. Vosoogh, and S. Maci, "Fundamental directivity limitations of dense array antennas: A numerical study using Hannan's embedded element efficiency," *IEEE Antennas Wireless Propag. Lett.*, vol. 15, pp. 766–769, 2016.
[65] P.-S. Kildal, *Foundations of Antenna Engineering: A Unified Approach for Line-of-Sight and Multipath*. Gothenburg, Sweden, Artech House, 2015.
[66] F. Yang and Y. Rahmat-Samii, *Electromagnetic Band Gap Structures in Antenna Engineering*. Cambridge, U.K.: Cambridge Univ. Press, 2009.
[67] M. F. Abedin and M. Ali, "Effects of EBG reflection phase profiles on the input impedance and bandwidth of ultrathin directional dipoles," *IEEE Trans. Antennas Propag.*, vol. 53, no. 11, pp. 3664–3672, Nov. 2005.
[68] F. Yang and Y. Rahmat-Samii, "Reflection phase characterizations of the EBG ground plane for low profile wire antenna applications," *IEEE Trans. Antennas Propag.*, vol. 51, no. 10, pp. 2691–2703, Oct. 2003.
[69] S. Jaeckel, L. Raschkowski, K. Börner, and L. Thiele, "QuaDRiGa: A 3-D multi-cell channel model with time evolution for enabling virtual field trials," *IEEE Trans. Antennas Propag.*, vol. 62, no. 6, pp. 3242–3256, Jun. 2014.
[70] 3GPP, "Study on channel model for frequencies from 0.5 to 100 GHz, version 16.1.0," 3GPP, Sophia Antipolis, France, Tech. Rep. 38.901, 2020. [Online]. Available: http://www.3gpp.org/dynareport/38901.htm

**Shuai S. A. Yuan** (Graduate Student Member, IEEE) received the B.Eng. degree from the Nanjing University of Aeronautics and Astronautics, Nanjing, China, in 2019. He is currently working toward the Ph.D. degree in electronic science and technology from Zhejiang University, Hangzhou, China. From 2023 to 2024, he was a visiting Ph.D. Student with ELEDIA Research Center, University of Trento, Trento, Italy. His main research interests include the electromagnetic methods for wireless communications, antenna arrays, and metasurfaces.

**Jie Wu** (Member, IEEE) was born in Anhui, China, in 1990. He received the B.S. degree in information and computing science from Anhui Jianzhu University, Hefei, China, in 2013, the M.S. degree from the Hefei University of Technology, Hefei, China, in 2018, and the Ph.D. degree in electromagnetic field and microwave technology from Anhui University, Hefei, in 2021. He is currently a Lecturer with the School of Electronic Engineering and Integrated Circuits, Hefei Normal University, Hefei. His research interests include orbital angular momentum antennas, mm-Wave antenna, and recongurable antennas.

**Hongjing Xu** received the Ph.D. degree from the Department of Electronic Engineering, Tsinghua University, Beijing, China, in 2021. She is a currently a Senior Engineer with Wireless Network System Technology Innovation Research Department, Huawei Technologies Company Ltd., Shanghai, China. Her research interests include MIMO antenna system design and reconfigurable intelligent surface.

**Tengjiao Wang** received the B.S. and Ph.D. degrees from the Department of Electronic Engineering, Tsinghua University, Beijing, China, in 2016 and 2021, respectively. He was a Visiting Scholar with the Massachusetts Institute of Technology, Cambridge, MA, USA, in 2019. He is currently a Principal Engineer with Radio Access Network Research Department, Huawei Technologies Company, Ltd., Shanghai, China. His research interests include 5G-Advanced wireless communications, visible light communications, and machine learning.

**Da Li** (Member, IEEE) received the B.S. and Ph.D. degrees in electrical engineering from Zhejiang University, Hangzhou, China, in 2014 and 2019, respectively. From 2017 to 2018, he was a Visiting Scientist with Nanyang Technological University, Singapore. From 2019 to 2021, he joined Science and Technology on Antenna and Microwave Laboratory, China, as a Research Fellow. He is currently an Assistant Professor with Zhejiang University. He has authored or coauthored more than 70 refereed papers. His research interests include machine learning, antennas, metasurfaces, and electromagnetic compatibility. He was a reviewer for six technical journals and TPC members of various IEEE conferences. He was the recipient of 2022 IEEE Motohisa Kanda Award, and Outstanding Young Scientist Award at 2022 Asia-Pacific International Symposium on Electromagnetic Compatibility. He was also the recipient of four Best Student Paper Prizes with his students.

**Xiaoming Chen** (Senior Member, IEEE) received the B.Sc. degree in electrical engineering from Northwestern Polytechnical University, Xi'an, China, in 2006, and the M.Sc. and Ph.D. degrees in electrical engineering from the Chalmers University of Technology, Gothenburg, Sweden, in 2007 and 2012, respectively. From 2013 to 2014, he was a Postdoctoral Researcher with the Chalmers University of Technology. From 2014 to 2017, he was with Qamcom Research and Technology AB, Gothenburg, Sweden. Since 2017, he has been a Professor with Xi'an Jiaotong University, Xi'an. He has authored or coauthored more than 200 journal articles on these topics. His research interests include MIMO antennas, over-the-air testing, and antenna measurements. Prof. Chen is currently the Track Editor of IEEE ANTENNAS AND WIRELESS PROPAGATION LETTERS and an Associate Editor for IEEE TRANSACTIONS ON ANTENNAS AND PROPAGATION. He was the General Chair of the IEEE International Conference on Electronic Information and Communication Technology 2021. He was the recipient of the IEEE outstanding Associate Editor awards five times from 2018 to 2023, and the URSI (International Union of Radio Science) Young Scientist Award 2017 and 2018.

**Chongwen Huang** (Member, IEEE) received the B.Sc. degree from Nankai University, Tianjin, China, in 2010, and the M.Sc. degree from the University of Electronic Science and Technology of China, Chengdu, China, in 2013, and the Ph.D. degree from the Singapore University of Technology and Design (SUTD), Singapore, in 2019. From October 2019 to September 2020, he was a Postdoc with SUTD. In September 2020, he joined Zhejiang University as a tenure-track young Professor. His main research interests include holographic MIMO surface/reconfigurable intelligent surface, B5G/6 G wireless communications, mmWave/THz communications, and deep learning technologies for wireless communications. Dr. Huang was the recipient of 2021 IEEE Marconi Prize Paper Award, 2023 IEEE Fred W. Ellersick Prize Paper Award, and 2021 IEEE ComSoc Asia-Pacific Outstanding Young Researcher Award. Since 2021, he has been an Editor of IEEE COMMUNICATIONS LETTER, ELSEVIER SIGNAL PROCESSING, EURASIP JOURNAL ON WIRELESS COMMUNICATIONS AND NETWORKING, and *Physical Communication*.

**Sheng Sun** (Senior Member, IEEE) received the B.Eng. degree in information engineering from Xi'an Jiaotong University, Xi'an, China, in 2001, and the Ph.D. degree in electrical and electronic engineering from Nanyang Technological University (NTU), Singapore, in 2006. From 2005 to 2006, he was with the Institute of Microelectronics, Singapore. From 2006 to 2008, he was a Postdoctoral Research Fellow with NTU. From 2008 to 2010, he was a Humboldt Research Fellow with the Institute of Microwave Techniques, University of Ulm, Ulm, Germany. From 2010 to 2015, he was a Research Assistant Professor with The University of Hong Kong, Hong Kong. Since 2015, he has been a Full Professor with the University of Electronic Science and Technology of China, Chengdu, China. He has authored or coauthored one book and two book chapters and more than 220 journal and conference publications. His research interests include electromagnetic theory, computational electromagnetics, multiphysics, numerical modeling of planar circuits and antennas, microwave passive and active devices, and microwaveand millimeter-wave communication systems. Dr. Sun was the recipient of the ISAP Young Scientist Travel Grant, Japan, in 2004, Hildegard Maier Research Fellowship of the Alexander Von Humboldt Foundation, Germany, in 2008, Outstanding Reviewer Award of IEEE Microwave and Wireless Components Letters in 2010, and the General Assembly Young Scientists Award from the International Union of Radio Science in 2014.

**Shilie Zheng** (Member, IEEE) received the B.S. and M.S. degrees in materials science and the Ph.D. degree in physical electronics and optoelectronics from Zhejiang University, Hangzhou, China, in 1995, 1998, and 2003, respectively. In 1998, she joined the Department of Information Science and Electronic Engineering, Zhejiang University, where she was appointed as an Associate Professor in 2005. From 2005 to 2006, she spent five months with Tohoku University, Sendai, Japan, as a Research Assistant. From 2016 to 2017, she was a Visiting Research Fellow with the RF and Microwave Laboratory, National University of Singapore, Singapore. In 2017, she was appointed as a Full Professor with Zhejiang University. Her research interests include twisted radio waves and applications, microwave photonics, and wireless communications.

**Xianmin Zhang** (Member, IEEE) received the B.S. and Ph.D. degrees in physical electronics and optoelectronics from Zhejiang University, Hangzhou, China, in 1987 and 1992, respectively. In 1994, he was appointed as an Associate Professor of information and electronic engineering with Zhejiang University, where he was a Full Professor, in 1999. He was a Research Fellow with The University of Tokyo, Tokyo, Japan, and Hokkaido University, Sapporo, Japan, from 1996 to 1997, and 1997 to 1998, respectively. In 2007, he spent two months with the Research Laboratory of Electronics, Massachusetts Institute of Technology, Cambridge, MA, USA, as a Visiting Research Fellow. From 2005 to 2017, he was the Dean of the Department of Information Science and Electronic Engineering, Zhejiang University, where he was the Dean of the School of Microelectronics, from 2015 to 2018, and the Vice Dean of the Polytechnic Institute, from 2016 to 2018. From 2018 to 2020, he was the President of the Ningbo Institute of Technology, Zhejiang University, Ningbo, China, where he was the Dean of Ningbo Campus, from 2018 to 2020. He is currently the Vice President of NingboTech University, Ningbo. His research interests include microwave photonics and electromagnetic wave theory and applications.

**Er-Ping Li** (Fellow, IEEE) received the Ph.D. degree in electrical engineering from Sheffield Hallam University, Sheffield, U.K., in 1992. Since 1989, he has been a Research Fellow, Principal Research Engineer, an Associate Professor, and the Technical Director of the Singapore Research Institute and University, Singapore. He is currently a Changjiang-Qianren Distinguished Professor with the Department of Information Science and Electronic Engineering and the Dean of the Joint Institute of Zhejiang University/University of Illinois at Urbana-Champaign, Zhejiang University, Hangzhou, China. He has authored or coauthored more than 500 articles published in the refereed international journals and conferences, and authored two books published by John-Wiley-IEEE Press and Cambridge University Press. He holds and has filed a number of patents at the U.S. patent office. His research interests include the electrical modeling and design of micro/nanoscale integrated circuits, 3-D electronic package integration, and nanoplasmonic technology. Dr. Li is a Fellow of the Singapore Academy of Engineering and the USA Electromagnetics Academy. He was the recipient of the IEEE Electromagnetic Compatibility Technical Achievement Award, in 2006, Singapore IES Prestigious Engineering Achievement Award, Changjiang Chair Professorship Award, in 2007, 2015 IEEE Richard Stoddard Award on EMC, 2021 IEEE EMC Laurence G. Cumming Award, and Zhejiang Natural Science First Class Award. From 2006 to 2008, he was an Associate Editor for IEEE MICROWAVE AND WIRELESS COMPONENTS LETTERS, and from 2006 and 2010, he was a Guest Editor of IEEE TRANSACTIONS ON ELECTROMAGNETIC COM Special Issue, and 2010 IEEE TRANSACTIONS ON MICROWAVE THEORY AND TECHNIQUES APMC Special Issue. He is currently an Associate Editor for IEEE TRANSACTIONS ON SIGNAL AND POWER INTEGRITY and the Executive Editor-in-Chief of *Electromagnetic Science*. He is the general chair and a technical chair for many international conferences. He was the President of 2006 International Zurich Symposium on EMC, Founding General Chair of Asia-Pacific EMC Symposium, and General Chair of 2008, 2012, 2016, 2018, 2022 APEMC, and 2010 IEEE Symposium on Electrical Design for Advanced Packaging Systems. He has been invited to give 120 invited talks and plenary speeches at various international conferences and forums.

**Wei E. I. Sha** (Senior Member, IEEE) received the B.S. and Ph.D. degrees in electronic engineering from Anhui University, Hefei, China, in 2003 and 2008, respectively. From 2008 to 2017, he was a Postdoctoral Research Fellow and then a Research Assistant Professor with the Department of Electrical and Electronic Engineering, The University of Hong Kong, Hong Kong. From 2018 to 2019, he was with University College London, London, U.K., as a Marie-Curie Individual Fellow. In October 2017, he joined the College of Information Science and Electronic Engineering, Zhejiang University, Hangzhou, China, where he is currently a tenured Associate Professor. He has authored or coauthored 200 refereed journal articles, 160 conference publications, ten book chapters, and two books. His Google Scholar citation is 9900 with an H-index of 51. His research interests include theoretical and computational research in electromagnetics, focusing on the multiphysics and interdisciplinary research. He was a Reviewer for 60 technical journals and a technical program committee member of ten IEEE conferences. He was the recipient of the Second Prize of Science and Technology from Anhui Province Government, China, in 2015, and Technical Achievement Award of Applied Computational Electromagnetics Society (ACES) in 2022. He was also the recipient of the seven best student paper prizes with his students. He was also an Associate Editor for IEEE JOURNAL ON MULTISCALE AND MULTI PHYSICS COMPUTATIONAL TECHNIQUES, IEEE OPEN JOURNAL OF ANTENNAS AND PROPAGATION, and IEEE ACCESS.